Life Sciences 217 (2019) 193–201

Contents lists available at ScienceDirect

Life Sciences

journal homepage: www.elsevier.com/locate/lifescie

# Water-soluble Ru(II)-anethole compounds with promising cytotoxicity toward the human gastric cancer cell line AGS

Eduardo Carrillo[a], Sebastián Ramírez-Rivera[b], Giuliano Bernal[b], Gisela Aquea[c], Catherine Tessini[d], Franz A. Thomet[a,*]

[a] Laboratory of Organometallics, Department of Chemistry, Universidad Técnica Federico Santa María, Avenida España N° 1680, Valparaíso, Chile
[b] Laboratory of Molecular and Cellular Biology of Cancer, Department of Biomedical Sciences, Faculty of Medicine, Universidad Católica del Norte, Larrondo N° 1281, Coquimbo, Chile
[c] Laboratory of Biological Chemistry, Institute of Chemistry, Faculty of Sciences, Pontificia Universidad Católica de Valparaíso, Brasil N° 2950, Valparaíso, Chile
[d] LabQI, Department of Chemistry, Universidad Técnica Federico Santa María, Avenida España N° 1680, Valparaíso, Chile

ARTICLE INFO

*Keywords:*
Organometallic Ru(II) compounds
Gastric cancer
Cytotoxic activity

ABSTRACT

*Aims:* Ruthenium-based compounds exhibit critical biochemical properties making them suitable for diverse pharmacological applications. The aim of this work was to study the anticancer effects of three ruthenium complexes on a human gastric cancer cell line.

*Main methods:* We synthetized three [Ru($\eta^6$-anethole)(en)X]$PF_6$ complexes, where (en) is ethylenediamine and X is Cl (**1**), Br (**2**) or I (**3**), which were then evaluated by MTT assay, RT-qPCR and flow cytometry on the human gastric cancer cell line AGS.

*Key findings:* Compound **3** exhibited the highest cytotoxicity ($IC_{50}$ = 11.27 ± 1.08 μM) of the series, with an activity almost three-fold more potent than the commercial drug cisplatin, and also revealed a 4.5-fold less potent cytotoxicity in the human normal gastric cell line GES-1. The exchange of the halogen (Cl, Br or I) on the organometallic compound slightly alters its solubility in PBS and lipophilicity (expressed as Log P). Studies of gene expression revealed that compound **3** induces a significant overexpression of the pro-apoptotic genes Caspase-3, PUMA and DIABLO in the gastric cancer cell line AGS after 6 h. In contrast, only PUMA was significantly overexpressed in the normal gastric cell line GES-1. Compound **3** induced the activation of multiple caspases in AGS cells: a sign of apoptosis. Characterization via single-crystal X-ray diffraction for compound **3** confirmed the key structural features for this type of organometallic complexes.

*Significance:* Our data suggests that compound **3** may be an interesting anticancer molecule for the treatment of gastric cancer.

## 1. Introduction

Gastric cancer (GC) is one of the principal causes of cancer deaths in the world, with 952,000 new cases and 723,000 deaths documented in 2012 [1]. Chile has one of the higher mortality rates for GC in the world: 18.72/100,000 individuals in 2015, and GC is the deadliest cancer in Chile with > 3300 deaths annually [2]. Currently, surgery with adjuvant chemotherapy and radiation therapy is the course of treatment for the majority of patients with advanced GC, but treatment options vary between patients. In those with HER2-positive tumors, trastuzumab combined with capecitabine, or 5-fluorouracil (FU) combined with cisplatin have shown to extend overall survival. For patients with HER2-negative tumors, combinations of two or three drugs: including irinotecan, docetaxel, oxaliplatin or 5-FU are effective treatment options for GC [3]. The use of docetaxel plus cisplatin and fluorouracil as a non-surgical first-line treatment option has shown better overall rates of survival as compared with cisplatin and fluorouracil alone, but side effects were notably higher with three drugs [4]. Platinum drugs are an effective treatment for several cancers, despite their side effects and sensitivity to resistance mechanisms. Therefore, it is necessary to develop new compounds with more potent antitumor activity and specificity against GC cells while reducing side effects [5].

Ruthenium-based compounds are among the most promising non-platinum therapeutics, due to their interesting biological properties. Ru (III) compounds like NAMI-A, KP1019 and NKP1339 (the sodium salt analogue of KP1019), have showed remarkable activity for in vitro and

* Corresponding author at: Universidad Técnica Federico Santa María, Avenida España N° 1680, Valparaíso, Chile.
*E-mail address:* franz.thomet@usm.cl (F.A. Thomet).

https://doi.org/10.1016/j.lfs.2018.12.010
Received 22 September 2018; Received in revised form 16 November 2018; Accepted 5 December 2018
Available online 06 December 2018
0024-3205/ 

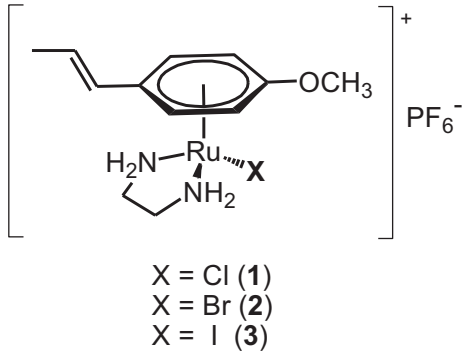


**Fig. 1.** Organometallic Ru(II)-anethole compounds employed in this study.

in vivo models, and have been tested in clinical trials [6]. Development of the organometallic Ru(II) "piano-stool" compounds have also demonstrated promising results [7]. Traditionally, *p*-cymene or biphenyl have been employed as an arene ligand to synthesize new organometallic compounds that have the aqueous solubility and stability needed for further biological assessments [8]. Our group has synthesized this type of organometallic compound containing phenylpropanoids, using methylisoeugenol and anethole as the arene ligands. [Ru($\eta^6$-anethole)(en)Cl]$PF_6$ **1** (en: ethylenediamine, Fig. 1) showed promising in vitro cytotoxic activity toward a human colonic tumor cell line (HT-29; $IC_{50}$ = 18 ± 3 μM). This activity was slightly improved with the iodide analogue [Ru($\eta^6$-anethole)(en)I]$PF_6$ **3** ($IC_{50}$ = 10 ± 2 μM) [9,10]. The present work focuses on the study of the anti-proliferative behavior of the compounds **1–3** on the gastric tumor cell line AGS, and comparing this with the activity of the commercial drug cisplatin. The aqueous parameters solubility and lipophilicity were measured to establish a potential correlation between these properties and the cytotoxicity of the compounds. The expression of pro and anti-apoptotic genes in cancerous (AGS) and normal (GES-1) gastric cells was studied and X-ray diffraction was used to characterize the structure of the most promising compound, [Ru($\eta^6$-anethole)(en)I]$PF_6$ (**3**).

## 2. Materials and methods

### 2.1. General considerations

[Ru($\eta^6$-anethole)(en)X]$PF_6$ X: Cl (**1**), Br (**2**) and I (**3**) were synthesized through the reaction of the respective dimeric compound [Ru($\eta^6$-anethole)$X_2$]$_2$ (X: Cl, Br or I) with 3.2 eq. of ethylenediamine in MeOH following the established procedure [9,10]. Recrystallization by slow diffusion of ether in a methanolic solution produced suitable crystalline species for the single-crystal X-ray diffraction study of compound **3**.

### 2.2. X-ray diffraction

The single-crystal diffraction intensity data of compound **3** was collected at T = 296 K using graphite monochromated Mo-Kα radiation (λ = 0.71073 Å), on a Bruker AXS APEXII diffractometer equipped with a CCD detector. Absorption corrections were applied using SADABS [11]. The structure was solved using SHELXT [12] and refined with the full-matrix least-squares method based on $F^2$ using SHELXL [13], running under the control of Olex2 GUI [14]. Crystallographic data and refinement parameters for compound **3** are summarized in Table 1. The preparation of materials for publication was performed on MERCURY [15] and ORTEP3 [16]. All non-hydrogen atoms were refined with anisotropic displacement parameters (ADP). Hydrogen atoms were placed in their geometrically idealized positions and refined using the riding model with default parameters. The absolute configuration for the molecule was determined by refinement with the Flack parameter [17].

**Table 1**
Crystallographic refinement data of the compound **3**.

| | |
|---|---|
| Empirical formula | Ru $C_{12}$ $H_{20}$ $N_2$ O I, P $F_6$ |
| Formula weight | 581.24 |
| Temperature (K) | 296 |
| Crystal system | Orthorhombic |
| Space group, Z | $P2_12_12_1$, 4 |
| *a* (Å) | 8.880(1) |
| *b* (Å) | 10.510(1) |
| *c* (Å) | 20.038(2) |
| *V* (Å$^3$) | 1870.2(4) |
| μ (mm$^{-1}$) | 2.633 |
| F(000) | 1120.0 |
| Crystal size (mm$^3$) | 0.35 × 0.23 × 0.12 |
| Radiation | Mo-Kα (λ = 0.71073 Å) |
| Index ranges | $-10 \le h \le 10$, $-12 \le k \le 12$, $-23 \le l \le 23$ |
| Reflections collected | 58,838 |
| Data/restraints/parameters | 3310/30/219 |
| Goodness-of-fit on F2 | 1.028 |
| Final R (I ≥ 2σ (I)) | R1 = 0.0303, wR2 = 0.0788 |
| Final R (all data) | R1 = 0.0341, wR2 = 0.0823 |
| $\Delta\rho_{max}/\Delta\rho_{min}$ (e Å$^{-3}$) | 0.54/−0.28 |
| Flack parameter | −0.012(17) |

### 2.3. Solubility determination

Solubility was determined using phosphate buffered saline (PBS). Sample in excess (5 mg) was added to 3 Eppendorf tubes containing 300, 400 and 500 μL of PBS, which were then sonicated for 10 min and held at 25 °C for at least 24 h in the absence of light. The samples were filtered and ruthenium content was determined by atomic absorption.

### 2.4. Lipophilicity determination

Log P values were determined using the shake-flask method [18]. The measurements were carried out at 25 °C, in triplicate for each compound.

In a 50 mL flask, 5 mL of octanol (saturated with 0.2 M HCl) was added to 5 mL of the aqueous solution (saturated with octanol) containing the ruthenium compound (approximately 2.5 mg). The flask was vortex shaken for 2 h then centrifuged at 3000 rpm for 10 min. It was left to settle for 24 h to allow for phase separation. Amount of ruthenium compound was determined by atomic absorption measurement of the aqueous phase (n = 4).

### 2.5. Atomic absorption method

An Agilent Technologies AA 240 flame atomic absorption spectrometer equipped with hollow cathode lamps was used to measure atomic absorption. Instrumental parameters were adjusted according to the manufacturer's recommendations. A Ru hollow cathode lamp operating at 349.9 nm was used, and the lamp current was set to 6.0 mA. The flame composition was $N_2O$-acetylene (11–50 psi).

The aqueous phase was digested in a heating plate (70–75 °C) using 3 mL of $HNO_3$/HCl (3:1 v/v). When cool, the residue was transferred to 10 mL volumetric flasks, 0.433 g of $La(NO_3)_3 * 6H_2O$ and 0.67 mL of HCl were added, and the solution was diluted with deionized water. Before analysis, samples were filtered through a 0.45 μm membrane filter. The samples were analyzed in quintuplicate.

### 2.6. Cell culture

The human GC cell line AGS (ATCC® CRL-1739™) was obtained from "Fundación Ciencia & Vida" (Chile), donated by Dr. Lorena Lobos-González and Dr. Luis Burzio, and maintained in Ham's F-12K (Kaighn's) culture medium (Corning). The medium was supplemented with 10% FBS, 100 units/mL penicillin G, and 100 μg/mL streptomycin.

Normal human gastric epithelial cells GES-1 were used as a control,

donated by Dr. Dawit Kidane-Mulat from the University of Texas-Austin. GES-1 cells were cultivated in DMEM culture medium (Corning), supplemented with 10% FBS, 100 units/mL penicillin G, and 100 µg/mL streptomycin. Cells were kept at 37 °C, 5% $CO_2$ in a humidified incubator.

### 2.7. Measurement of cell viability

Cells were seeded to a density of 5000 cells/well in 96-well plates with F12-K medium and treated with different concentrations of ruthenium compounds **1–3** (0.78, 1.5, 3.1, 6.25, 12.5, 25, 50, and 100 µM) for 24 h. Cell viability was determined by MTS reduction assay, first adding 20 µL of CellTiter 96® $AQ_{ueous}$ One Solution Cell Proliferation Assay System (Promega) to each well and then incubating for 2 h. Stock solutions of the complexes were prepared in DMSO, and in all experiments the concentration of DMSO was maintained at 0.1%. Absorbance measurements were made in a NOVOstar 700-0130 at 490 nm. Cisplatin treatment was used as a control.

Cellular viability was calculated as:

$$\%\text{Cell viability} = \frac{\text{OD treatment}}{\text{OD control}} \times 100$$

The formula to calculate $IC_{50}$ was:

$$Y = \text{Bottom} + (\text{Top}-\text{Bottom})/(1 + 10\text{^}((\text{Log}IC_{50} - X)*\text{Hill Slope}))$$

where X = log of concentration; Y = normalized response; Hill Slope: slope factor.

### 2.8. Determination of gene expression

#### 2.8.1. RNA extraction and Reverse Transcription

$5 \times 10^6$ cells were treated with 12.5 or 25 µM of [Ru($\eta^6$-anethole)(en)l]$PF_6$ (**3**) for 6 h. RNA was extracted from the cells using the SV Total RNA Isolation System kit (Promega®), according to the manufacturer's instructions. Later 500 ng of RNA was used to synthesize cDNA by Reverse Transcription with Affinity Script II (Agilent®).

#### 2.8.2. Gene expression analysis by qPCR

The response in apoptotic and anti-apoptotic gene expression to [Ru($\eta^6$-anethole)(en)l]$PF_6$ (**3**) treatment was evaluated. To do so, 2 µL of cDNA was used to measure the expressions of the genes Bcl-xL, Bcl-2, Bax, DIABLO, PUMA, and Caspase-3. B2M was used as a housekeeping gene. The qPCR mix contained 5 µL of SYBR Kapa 2x, and 0.1 µM of each primer, in a final volume of 10 µL. Thermocycling conditions were as follows: denaturation at 95 °C for 10 min, followed by 35 amplification cycles at 95 °C for 10s, and 30s at the primer's annealing temperature. Primers for each gene are shown in Table 2.

**Table 2**
Primers used for RT-qPCR.

| Gene | Sequence | Amplicon size |
|---|---|---|
| Bax | FP- 5′-CTC ACC GCC TCA CTC ACC AT-3′<br>RP- 5′-TGT GTC CCG AAG GAG GTT TAT TT-3′ | 201 bp |
| Caspase-3 | FP- 5′-GAG TAG ATG GTT TGA GCC TGA G-3′<br>RP- 5′-TGC CTC ACC ACC TTT AGA AC-3′ | 205 bp |
| Bcl-2 | FP- 5′-TGA GTA CCT GAA CCG GCA CC-3′<br>RP- 3′-GGG CCA AAC TGA GCA GAG TC-3′ | 140 bp |
| Bcl-xL | FP- 5′-TCG GAT CGC AGC TTG GAT GG-3′<br>RP- 5′-GAA GCG TTC CTG GCC CTT TC-3′ | 139 bp |
| PUMA | FP- 5′-GAC CTC AAC GCA CAG TAC GA-3′<br>RP- 5′-GAG ATT GTA CAG GAC CCT CCA-3′ | 84 bp |
| DIABLO | FP- 5′-TAA CCC TGT GTG CGG TTC CT-3′<br>RP- 5′-ACC AAA GAC ACT GCT CTC CTC AT-3′ | 88 bp |

### 2.9. Analysis of apoptosis by flow cytometry

#### 2.9.1. Annexin-V and Dead Cell assay

AGS cells were seeded to a cell density of $2 \times 10^5$ in F12-K medium, in six-well plates, for 24 h and then treated with either 12.5 or 25 µM of [Ru($\eta^6$-anethole)(en)l]$PF_6$ (**3**) for 48 h. Cisplatin 35 µM was used as a positive control and untreated cells as a negative control. All wells contained 0.1% DMSO. Cells were washed with PBS 1×, detached using trypsin, and then resuspended in F12-K media with 1% FBS. The Muse Annexin-V & Dead Cell Assay kit (EMD Millipore Bioscience) was used to quantify apoptotic cells, according to the manufacturer's instructions. Briefly, 100 µL of cells was aliquoted into 1.5 mL microcentrifuge tubes and 100 µL of Muse™ Annexin-V & Dead Cell reagent was added to the cells, then incubated for 20 min at room temperature in the dark. The kit uses a fluorescent marker (FITC) conjugated with Anexin-V to detect phosphatidylserine (PS) in the external membrane of apoptotic cells, and 7-AAD (7-Aminoactinomycin D), which has a strong affinity for DNA, to mark cell death. The Muse™ Cell Analyzer flow cytometer (Merck Millipore, USA) was used to measure changes in cell viability.

#### 2.9.2. MultiCaspase assay

AGS cells were treated as described. Detection of the activation of multiple caspases (caspase-1, 3, 4, 5, 6, 7, 8 and 9) was performed with Muse™ MultiCaspase Assay Kit (Merck Millipore, USA), following the manufacturer's instructions. Fifty microliters (50 µL) of treated cells and 5 µL of Muse™ MultiCaspase reagent working solution were combined in 1.5 mL microcentrifuge tubes and incubated for 30 min at 37 °C. After, 150 µL of Muse™ caspase 7-aminoactinomycin D (7-AAD) working solution was added to each tube and mixed and left for 5 min at room temperature in the dark. The percentage of cells with multiple caspase activity was measured using the Muse™ cell analyzer (Merck Millipore, USA) flow cytometer.

### 2.10. Statistical analysis

All data was analyzed with GraphPad Prism 6 Software and expressed as the mean ± standard deviation of three measurements. Statistical comparisons were made by ANOVA, and the non-parametric Kruskall-Wallis test followed by Dunn's multiple comparison test. P-values lower than 0.05 ($P < 0.05$) were considered significant.

## 3. Results and discussion

### 3.1. Single-crystal X-ray structure analysis of [Ru($\eta^6$-anethole)(en)I]$PF_6$ (3)

Fig. 2 shows the molecular structure of the [Ru($\eta^6$-anethole)(en)I]$^+$ cationic complex with an atomic numbering scheme. It shows the classical 'piano-stool' geometry expected for this kind of compound. A single molecule of the asymmetric unit is shown. Selected bond lengths and angles are listed in Table 3. The C8—C9 (double bond), Ru—N, and Ru—Cnt (Cnt: centroid of the C1–C6 aromatic ring) distances are in agreement with those reported for the analogous [Ru($\eta^6$-anethole)(en)Br]$PF_6$ compound [10]. Furthermore, the C4—C8—C9—C10 dihedral angle (representing the displacement between the C9—C10 atoms and the mean plane of the aromatic ring) and the N1—C11—C12—N2 dihedral angle (corresponding to the bridge of the ethylenediamine ligand) are comparable to the reported brominated analog [10]. The N1—Ru1—N2 bond angle (78.2(3)°) is slightly smaller than that found for similar compounds containing a ethylenediamine chelating ligand such as [Ru($\eta^6$-anethole)(en)Br]$PF_6$, [Ru($\eta^6$-methylisoeugenol)(en)Cl]$PF_6$, [Ru($\eta^6$-*p*-cymene)(en)Cl]$PF_6$ and [Ru($\eta^6$-biphenyl)(en)Cl]$PF_6$, which ranged from 78.78(9)° to 79.2(2)° [9,10,19]. The ADP's of the N2 and C12 atoms in the ethylenediamine ligand (Fig. 2) seem to be abnormally elongated. We tried to model them as disorder, but we get

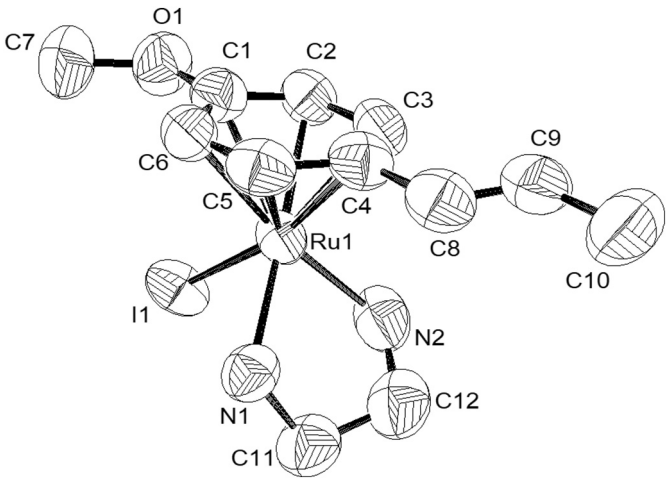


**Fig. 2.** ORTEP diagram of [Ru($\eta^6$-anethole)(en)I]$^+$ complex. Thermal ellipsoids are drawn at the 50% probability level. Hydrogen atoms were omitted for simplicity.

**Table 3**
Selected bond lengths [Å] and angles (°).

| | |
|---|---|
| Ru1−N1 | 2.139(7) |
| Ru1−N2 | 2.140(8) |
| Ru1−I1 | 2.7117(9) |
| Ru1−Cnt | 1.68(1) |
| C8−C9 | 1.28(1) |
| N1−Ru1−N2 | 78.4(3) |
| C4−C8−C9−C10 | 178.5(8) |
| N1−C11−C12−N2 | −54.0(1) |

**Table 4**
Solubility, lipophilicity, and cytotoxic activity (expressed as $IC_{50}$ values) against the gastric cancer cell line AGS and normal gastric cells GES-1 for compounds **1–3** and cisplatin.

| Compound | Solubility (mM) | Log P[a] | $IC_{50}$ (μM)[b] | |
|---|---|---|---|---|
| | | | AGS | GES-1 |
| **1** (Cl) | 11.5 ± 1.1 | −1.39 ± 0.04 | 71.71 ± 1.86 | – |
| **2** (Br) | 11.2 ± 1.2 | −1.15 ± 0.36 | 60.23 ± 1.77 | – |
| **3** (I) | 9.3 ± 0.7 | −1.00 ± 0.02 | 11.27 ± 1.08 | 50.93 ± 1.69 |
| Cisplatin | – | – | 32.50 ± 3.50 | 22.34 ± 1.11 |

[a] $P = []_{org}/[]_{aq}$.
[b] MTS assay after 24 h. Each value is the mean ± SD of three independent experiments.

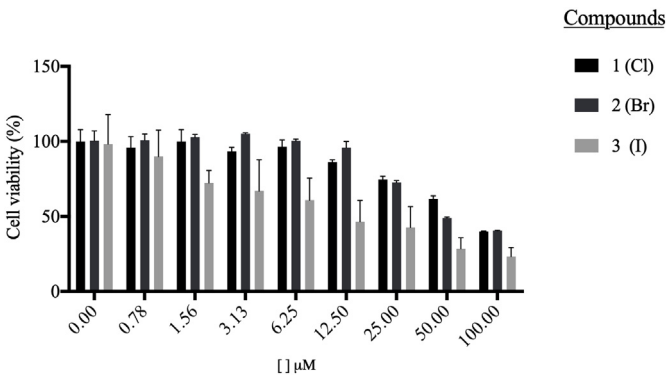


**Fig. 3.** Effect of compounds **1–3** on cell viability in the human gastric cancer cell line AGS after 24 h. Each measurement is the mean ± standard deviation. Error bars were calculated from three independent experiments.

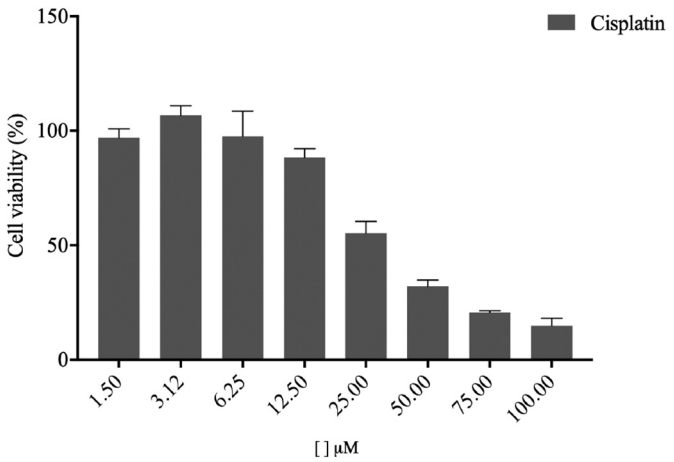


**Fig. 4.** Changes in cell viability induced by cisplatin on AGS cells were determined in vitro at 24 h. Each point is the mean ± standard deviation. Standard deviation was calculated from three independent experiments.

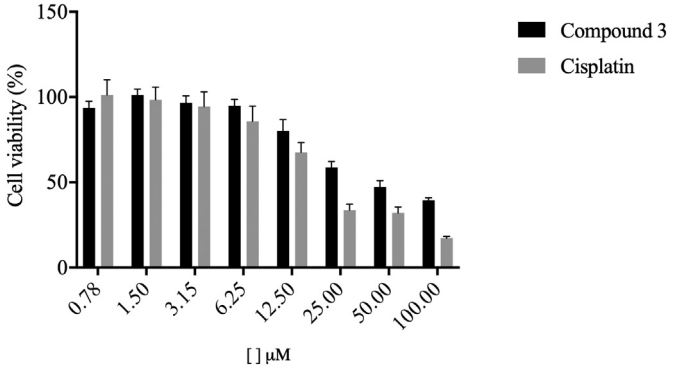


**Fig. 5.** Effect of compound **3** on cell viability for the human normal gastric cell line GES-1 after 24 h. Each measurement is the mean ± standard deviation. Error bars were calculated from three independent experiments. Cisplatin was used as a control.

only adequate ADP's when the bond lengths were chemically irrational. Finally, with the aid of the SIMU restrain, we decided that the elongated ADP's of those atoms were a better description, considering the fact that the data collection was made at room temperature. The cationic compound is complemented by a $PF_6^-$ counter-ion; the P−F bond lengths (ranging from 1.511(8) to 1.587(7)) are similar to those reported for the compound from the same family [10].

Intermolecular hydrogen-halogen interactions are present in the macromolecular crystal packing structure (Table 5, Supplementary material). The [Ru($\eta^6$-anethole)(en)I]$^+$ cations are connected by N−H…I bonds forming an infinite chain describing a C(4) motif [20]. Simultaneously, they are connected to $PF_6^-$ anions through N−H…F close contacts, whose graph set is $C_2^2(8)$ [20]. The presence of N2−H2B hydrogen bonding to F1 and F4 results in a $R_1^2(4)$ motif (Fig. 9, Supplementary material) [20]. The three-dimensional structure is defined by a zigzag chain running nearly parallel to the plane between the aromatic rings and the *c*-axis, as shown in Fig. 10 (see Supplementary material).

### 3.2. Solubility and lipophilicity determination

The organometallic Ru(II) compounds possess an appropriate balance between lipophilicity and hydrophilicity, allowing the complex to cross the cell membrane while maintaining appropriate plasma and intracellular concentrations. Solubility and lipophilicity vary significantly depending on the nature of the metal ion, the nature of the

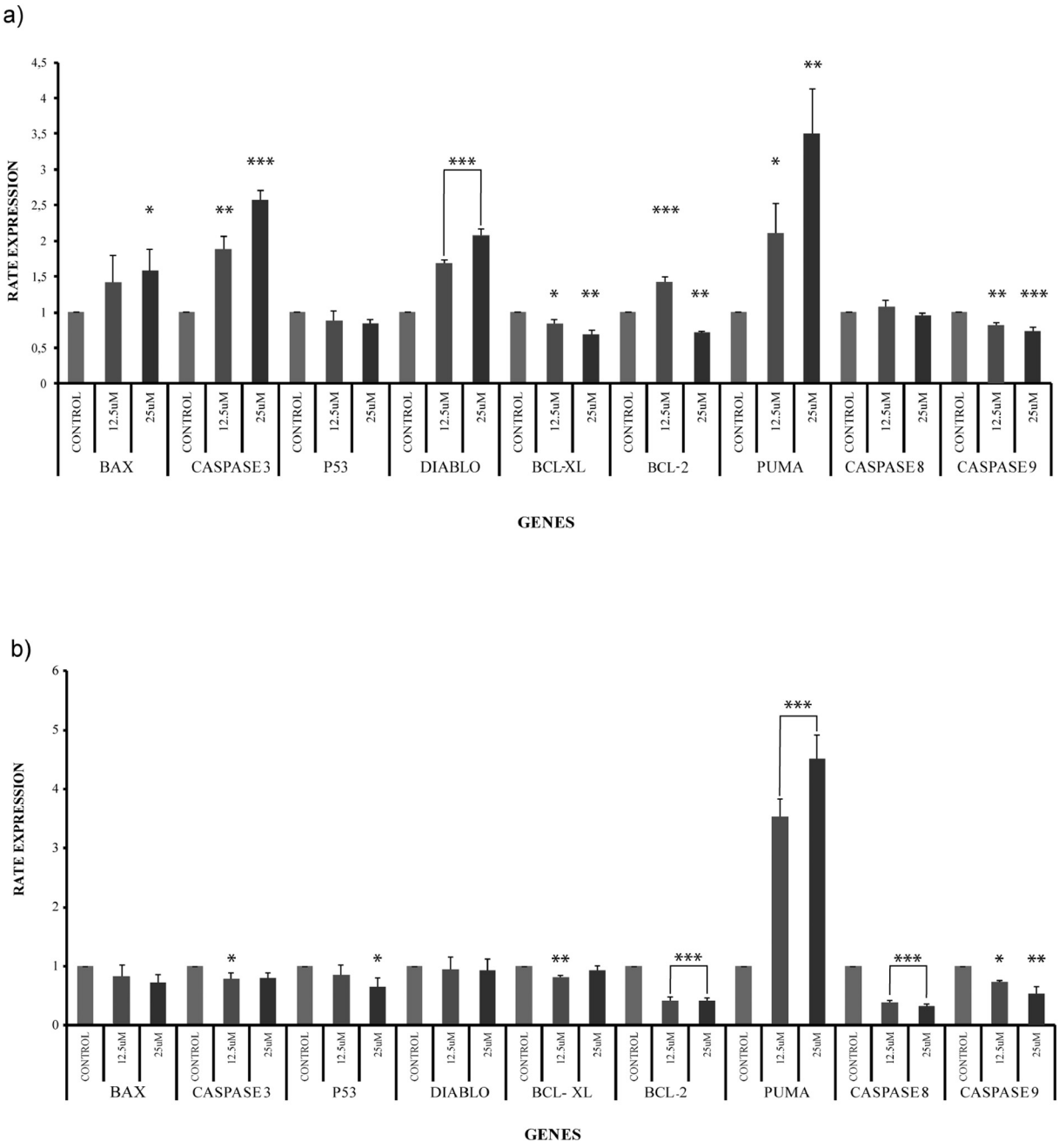


**Fig. 6.** Gene expression of gastric cells determined by RT-qPCR. Gene expression of Bax, Caspase-3, p53, Diablo, Bcl-xl, Bcl-2, Puma, Caspase 8 and Caspase 9 after 6 h with 12.5 μM or 25 μM of compound **3**: a) in gastric cancer cells AGS b) in gastric normal cells GES-1. Data is presented as the mean ± standard deviation. *P < 0.05, **P < 0.01, ***P < 0.005.

coordinated ligands, whether the compound is neutral or charged, and the counterion (for charged complexes) [21]. The solubility and lipophilicity of the synthesized organometallic Ru(II) compounds **1–3** were determined experimentally to evaluate the effect of the halogen, and to establish possible correlations between these physicochemical properties and cytotoxic activity. The solubility of the compounds in PBS (pH 7.4) showed that compound **3** is slightly less soluble than **1** and **2**, and no statistically significant difference was observed between compounds **1** and **2** (Table 4). The exchange of the halogen does not significantly affect the solubility of the organometallic Ru(II)-anethole compounds.

The determination of the lipophilicity of ionic compounds, as for the studied compounds **1–3**, is a more complex process as compared to that of neutral compounds. The partition ratio between the organic and the aqueous phase of cationic compounds depends on the cationic distribution ratio and also on the anionic distribution ratio [22]. Despite these challenges, the executed procedure allowed us to estimate an approximate value and compare the lipophilicity of the studied compounds **1–3**. The measurements (Table 4) show that the lipophilicity of compound **3** is slightly enhanced as compared to **1**. The less polarizing metal-halogen bond in compound **3** and the bulky nature of iodine favor the solubility of the organometallic compound in a nonpolar medium. This result is concordant with reported log P values for aminoflavone and aminochromone organometallic Ru(II) compounds, where iodide compounds showed a slightly enhanced lipophilicity as compared to chloride analogues [23].

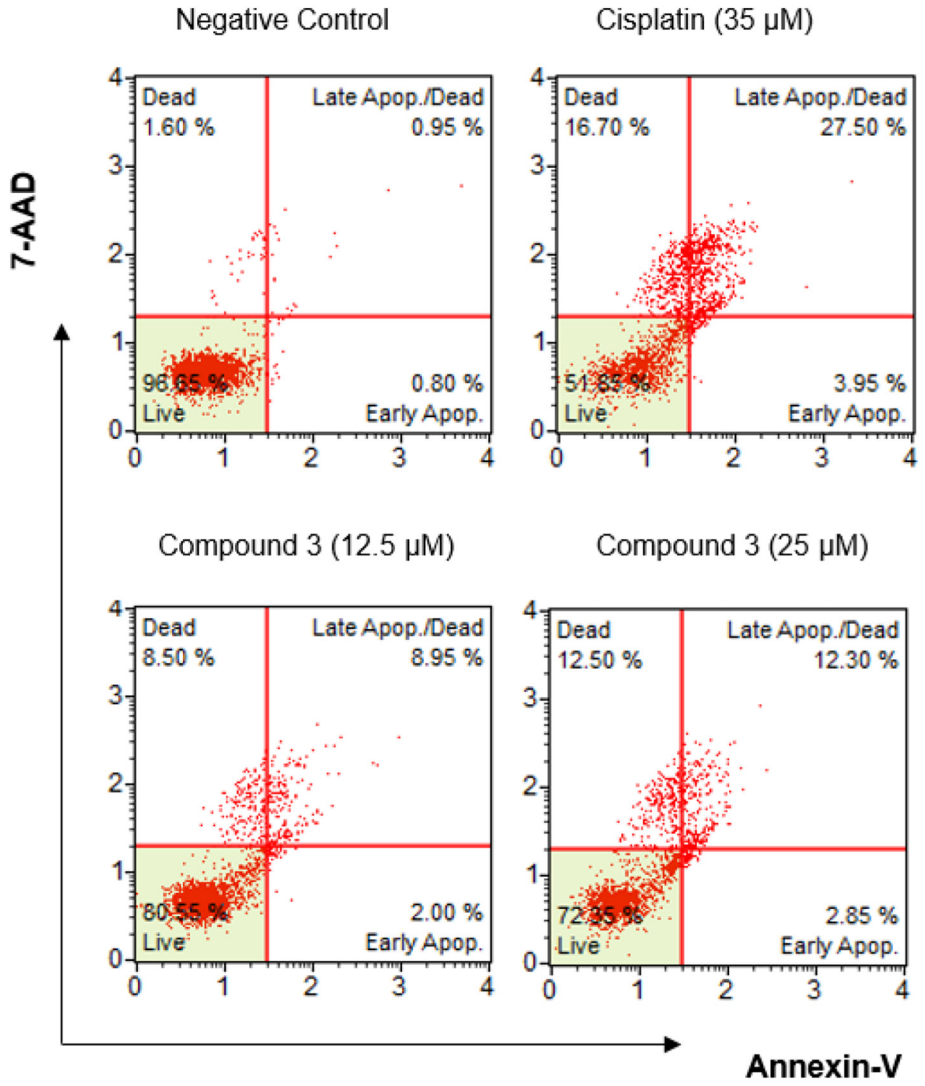


**Fig. 7.** The growth inhibitory effect of compound **3** on AGS cells is mediated by apoptosis. AGS cells were treated with 12.5/25 μM of compound **3** or 35 μM cisplatin, for 48 h and apoptosis was analyzed by flow cytometry after staining with FITC-annexin-V/7-AAD. The scattered blots show the percentages of early and late apoptosis; live and dead cells.

### *3.3. Cell viability*

The anti-proliferative activity of the ruthenium compounds **1**–**3** and cisplatin were determined on the human gastric cancer cell line AGS and normal gastric cells GES-1 after 24 h by MTS assay. All three ruthenium compounds inhibit cell proliferation in a dose-dependent manner, as is shown in Fig. 3, and $IC_{50}$ values are provided in Table 4. In AGS cells, the cytotoxicity of the series showed a clear halogenic effect as follows: **1** (71.71 ± 1.86 μM, less active) < **2** (60.23 ± 1.77 μM) < **3** (11.27 ± 1.08 μM, more active). A previous report established that compound **3** hydrolyses to a lower extent (24%) as opposed to compounds **1** and **2** (64% and 55% respectively) after 24 h [10], therefore enhanced anti-proliferative activity may be correlated with the higher aqueous stability of compound **3**. This trend in hydrolysis activity (**3** < **2** < **1**) differs from other ruthenium compounds when the three analogues (Cl, Br and I) were synthesized [24]. In contrast, Table 4 shows that compound **3** exhibited enhanced lipophilicity as compared to compound **1**, and this key physicochemical property may explain the potency of compound **3**. Our results are in agreement with the previously reported study of iodide vs chloride analogues for $[Ru(\eta^6\text{-}p\text{-cymene})(ImpyNMe_2)X]PF_6$ ($ImpyNMe_2$: iminopyridine-$NMe_2$; X: Cl or I), where again iodide compounds were more potent than chloride analogues [25]. Iodide accumulates ~60% more than the chloride analogue in the human ovarian carcinoma A2780 cell line after 24 h of exposure. Uptake of organometallic Ru(II) compounds is partly mediated by a passive diffusion process, especially for the iodide compound [26]. Hence, the higher aqueous stability in combination with enhanced lipophilicity of compound **3** may explain its superior biological activity against AGS cells. It is encouraging that compound **3** exhibited an anti-proliferative activity almost triple that of the commercial drug cisplatin, making it an important compound for continuing study (Fig. 4).

The measured cytotoxic activity of compound **3** on the normal gastric cell line GES-1 (Fig. 5) revealed an $IC_{50}$ = 50.93 ± 1.69 μM. This value indicates that compound **3** is almost five times less cytotoxic to the normal cell line than to the GC cells AGS. This is very important, because this result indicates that this compound could be more inclined to act against GC cells than normal gastric cells. Such selectivity (tumoral vs normal cell line) was not observed for the commercial drug cisplatin; it exhibited greater cytotoxic activity against the normal gastric cell line GES-1 (Table 4).

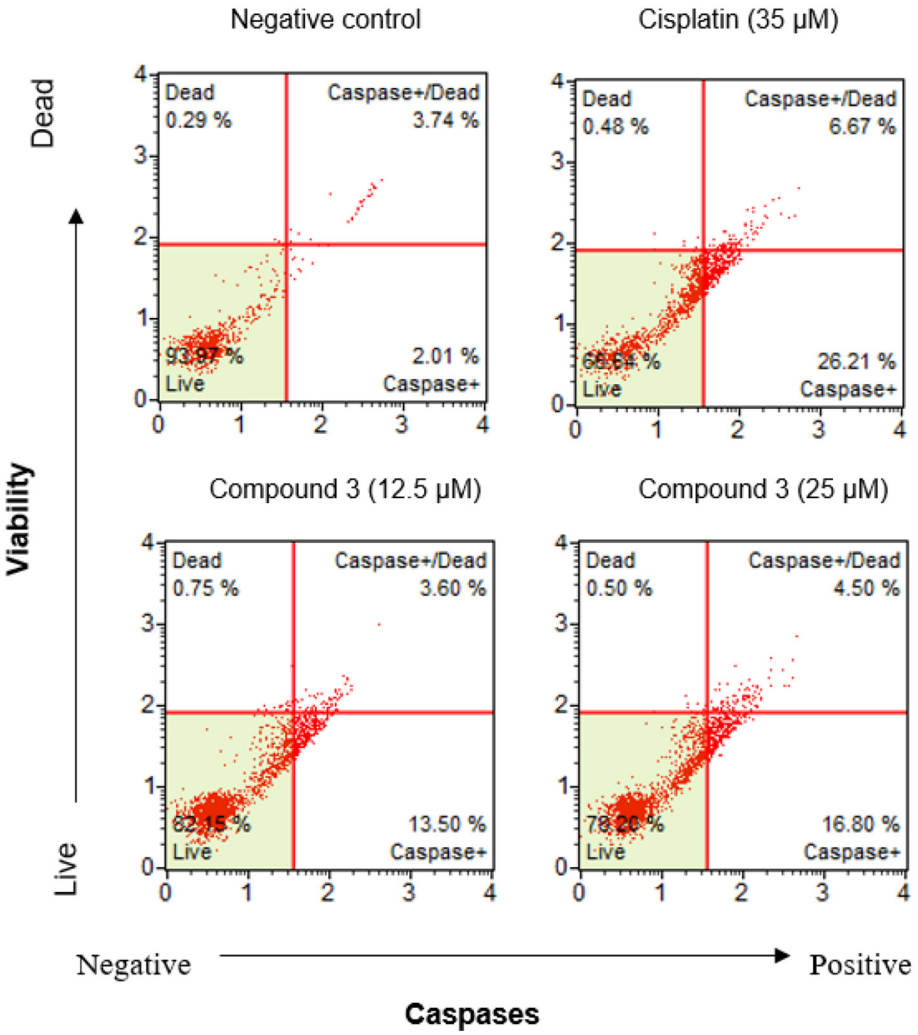


**Fig. 8.** Muse™ MultiCaspase assay. AGS cells treated with 12.5/25 μM of compound **3** or 35 μM of cisplatin, for 48 h were analyzed by flow cytometry.

### *3.4. Compound **3** induces the expression of pro-apoptotic genes*

We tested the effects of compound **3** at 12.5 and 25 μM for 6 h on apoptotic gene expression in AGS and GES-1 cells via RT-qPCR. As seen in Fig. 6a), significant overexpression of the pro-apoptotic genes Caspase-3, PUMA and DIABLO was observed with both concentrations of compound **3**. Moreover, a slight increase in the expression of Bax was observed. We did not observe a large repression in the expression of the anti-apoptotic genes Bcl-xL or Bcl-2 as was expected, and with 12.5 μM of compound **3** we even observed a small increase in Bcl-2 expression. Nevertheless, with 25 μM of this compound, the Bax/Bcl-2 ratio increased, which is to be expected for an antitumor drug. These molecules are critical in the cell death process, and the ratio of Bax/Bcl-2 is a deciding factor in the apoptotic pathway [27].

When normal gastric cells GES-1 were treated with compound **3**, only PUMA showed a significant overexpression, increasing 3–4 fold for both concentrations of compound **3** (Fig. 6b). The expression of the anti-apoptotic gene Bcl-2 was repressed by ~50% when treated with the organometallic compound, however expression of Bax, Caspase-3, DIABLO and Bcl-xL was not affected. These results indicate that compound **3** does not pose a danger to normal cells and its activity is specific toward cancer cells.

Expression of caspase-3 was mirrored in AGS cells with both treatments of compound **3**, but in GES-1 caspase-3 expression remained unchanged (Fig. 6). This protease is a key apoptotic factor and is directly activated by caspase-8, 9 and 10 in both the extrinsic and intrinsic pathways to initiate cell death [28,29]. Various studies have demonstrated that caspase-3 expression is repressed in GC tissues as compared to healthy gastric tissues [28,30,31]. Moreover, caspase-3 expression levels are higher in well-differentiated tumors as opposed to in poorly differentiated lesions. Apoptosis is greater in tumors with active caspase-3, which indicates that the expression of caspase-3 promotes apoptosis of tumor cells. Overexpression and activation of caspase-3 are desirable actions in antitumor drugs.

PUMA and DIABLO are the other pro-apoptotic genes that overexpressed when AGS cells were treated with compound **3** (Fig. 6a), which was expected because both genes are important in GC progression [32,33]. PUMA has a fundamental role in apoptosis by the p53-dependent and independent pathway in several human cancer tissues, including GC [33], whereas DIABLO binds to Inhibitor of Apoptosis Proteins (IAPs), blocking their caspase inhibiting activities and consequently increasing caspase activation [34].

In summation, we show that compound **3** triggered an apoptosis induction profile different in the gastric cancer cell line AGS as compared to the normal gastric cell line GES-1, and these differences may explain the 5-fold augment in cytotoxicity for compound **3** against gastric cancer cells.

### *3.5. The anti-proliferative effect of compound **3** is mediated by apoptosis*

As shown in Fig. 7, a dose-dependent increase in annexin-V + cells was observed after treating AGS cells with compound **3** for 48 h.

Quantitative measurement showed a proportional increase in the percentage of apoptotic AGS cells from 1.75% (control) to 10.95% and 15.15% after treatment with 12.5 μM and 25 μM, respectively. Meanwhile, 35 μM of cisplatin induced apoptosis in 31.45% of cancer cells. Later, cells with activated caspases were quantified with the Muse™ MultiCaspase assay, which clearly demonstrated that an increase in concentration of compound **3** correlates with an increase in cells with active caspases (Fig. 8). Non-treated cells showed caspase activation in 5.75% of cells, while compound **3** induced caspase activation in 17.10% and 21.30% of cells with treatments of 12.5 and 25 μM, respectively. As a positive control we used 35 μM of cisplatin, which induced activation of caspases in 32.88% of cells. These results show clearly that compound **3** is able to induce the activation of caspase-1, 3, 4, 5, 6, 7, 8, and 9, some of which participate in the apoptosis process as initiators (caspase-1, 4, 5, 8 and 9) and others as executioners (caspase-3, 6 and 7).

## 4. Conclusions

Measuring the cytotoxicity of the organometallic compounds [Ru($\eta^6$-anethole)(en)X]$PF_6$, where X = Cl (**1**), Br (**2**) or I (**3**), against the human gastric cancer cell line AGS reveals that compound **3** possesses interesting antitumoral activities. It exhibited a cytotoxic activity ($IC_{50}$ = 11.27 ± 1.08 μM) almost three times more potent than the commercial drug cisplatin ($IC_{50}$ = 32.50 ± 3.50 μM). Moreover, compound **3** also showed selectivity toward gastric cancer cells, as it was 4.5 times less cytotoxic toward the human normal gastric cell line GES-1 ($IC_{50}$ = 50,93 ± 1,69 μM). The commercial drug cisplatin exhibited a more toxic effect against the normal GES-1 cells. In relation to the aqueous properties of the compounds, the study showed that the exchange of the halogen on the organometallic compound did not have a significant effect on solubility in PBS. [Ru($\eta^6$-anethole)(en)I]$PF_6$ (compound **3**) exhibited a slightly enhanced lipophilicity compared to the chloride analog **1** and this physicochemical property often correlates with enhanced biological activity. The changes in gene expression affected by compound **3** after 6 h showed significant overexpression of the pro-apoptotic genes Caspase-3, PUMA and DIABLO in the gastric cancer cell line AGS. However, in the normal gastric cell line GES-1, only PUMA shows significant overexpression, and other important pro-apoptotic genes maintained normal expression levels. This data concurs with results of the multicaspase assay performed with compound **3** in AGS cells, indicating that this molecule induces apoptosis in cancer cells which is a highly sought characteristic for antitumor drugs. Single-crystal X-ray diffraction of compound **3** confirmed the classical 'piano-stool' geometry that was expected, as well as the main structural features common for this sort of compound. The complete characterization of this promising compound is now available.

## Conflict of interest statement

The authors declare that there are no conflicts of interest.

## Acknowledgments

The authors are thankful to the Universidad Técnica Federico Santa María (DGIIP 116.13.1) and CORFO 14IDL2-30087 grant for their financial support. Eduardo Carrillo is grateful to Dr. Andres Vega and Ms. Poldie Oyarzún from the Universidad Andres Bello for providing the Single-Crystal X-ray Diffractometer facility, and Dr. Raúl Cardoso for his valuable contribution in the crystallography analysis. Dr. Giuliano Bernal thanks Dr. Lorena Lobos-González, Dr. Luis Burzio and Dr. Dawit Kidane-Mulat, who kindly donated the cells for this work.

## Appendix A. Supplementary data

The supplementary material for this article can be found online free of charge. All supplementary crystallographic data for compound **3** is available from the CCDC database (accession number: 1816888). This data can be obtained for free at http://www.ccdc.cam.ac.uk/conts/retrieving.html or from the Cambridge Crystallographic Data Centre, 12 Union Road, Cambridge CB2 1EZ, UK; fax: (+44) 1223 336 033; or via e-mail: deposit@ccdc.cam.ac.uk. Supplementary data to this article can be found online at https://doi.org/10.1016/j.lfs.2018.12.010.

## References

[1] GLOBOCAN (IARC), Stomach cancer estimated incidence, mortality and prevalence worldwide, Available from: globocan.iarc.fr/old/FactSheets/cancers/stomach-new.asp.
[2] DEIS. Departamento de Estadísticas e Información de Salud. Ministerio de Salud, Available from: http://www.deis.cl/series-y-graficos-de-mortalidad/.
[3] A.D. Wagner, N.L.X. Syn, M. Moehler, W. Grothe, W.P. Yong, B.C. Tai, et al., Chemotherapy for advanced gastric cancer, Cochrane Database Syst. Rev. (8) (2017) CD004064, , https://doi.org/10.1002/14651858.CD004064.pub4.
[4] E. Van Cutsem, X. Sagaert, B. Topal, K. Haustermans, H. Prenen, Gastric cancer, Lancet 388 (2016) 2654–2664.
[5] A. Bergamo, C. Gaiddon, J.H. Schellens, J.H. Beijnen, G. Sava, Approaching tumour therapy beyond platinum drugs: status of the art and perspectives of ruthenium drug candidates, J. Inorg. Biochem. 106 (2012) 90–99.
[6] R. Trondl, P. Heffeter, C.R. Kowol, M.A. Jakupec, W. Berger, B.K. Keppler, NKP-1339, the first ruthenium-based anticancer drug on the edge to clinical application, Chem. Sci. 5 (2014) 2925–2932.
[7] A.A. Nazarov, C.G. Hartinger, P.J. Dyson, Opening the lid on piano-stool complexes: an account of ruthenium(II)-arene complexes with medicinal applications, J. Organomet. Chem. 751 (2014) 251–260.
[8] P. Zhang, P.J. Sadler, Advances in the design of organometallic anticancer complexes, J. Organomet. Chem. 839 (2017) 5–14.
[9] R.A. Delgado, A. Galdamez, J. Villena, P.G. Reveco, F.A. Thomet, Synthesis, characterization and in vitro biological evaluation of [Ru($\eta^6$-arene)(N,N)Cl]$PF_6$ compounds using the natural products arenes methylisoeugenol and anethole, J. Organomet. Chem. 782 (2015) 131–137.
[10] D. Astudillo, A. Galdámez, M.E. Sanguinetti, J. Villena, F.A. Thomet, Cytotoxic organometallic [Ru($\eta^6$-anethole)(en)(X)]$PF_6$ (X = Br or I) complexes: synthesis, characterization and in vitro biological evaluation, Inorg. Chem. Commun. 84 (2017) 221–224.
[11] Bruker, SADABS, Bruker AXS Inc., Madison, Wisconsin, USA, 2008.
[12] G.M. Sheldrick, SHELXT–integrated space-group and crystal-structure determination, Acta Crystallogr. A 71 (2015) 3–8.
[13] G.M. Sheldrick, Crystal structure refinement with SHELXL, Acta Crystallogr. C 71 (2015) 3–8.
[14] O.V. Dolomanov, L.J. Bourhis, R.J. Gildea, J.A. Howard, H. Puschmann, OLEX2: a complete structure solution, refinement and analysis program, J. Appl. Crystallogr. 42 (2009) 339–341.
[15] (a) C.F. Macrae, I.J. Bruno, J.A. Chisholm, P.R. Edgington, P. McCabe, E. Pidcock, et al., Mercury CSD 2.0–new features for the visualization and investigation of crystal structures, J. Appl. Crystallogr. 41 (2008) 466–470;
(b) C.F. Macrae, P.R. Edgington, P. McCabe, E. Pidcock, G.P. Shields, R. Taylor, et al., Mercury: visualization and analysis of crystal structures, J. Appl. Crystallogr. 39 (2006) 453–457.
[16] L.J. Farrugia, WinGX and ORTEP for Windows: an update, J. Appl. Crystallogr. 45 (2012) 849–854.
[17] H.D. Flack, On enantiomorph-polarity estimation, Acta Crystallogr. A 39 (1983) 876–881.
[18] Y. Qiao, S. Xia, P. Ma, Octanol/water partition coefficient of substituted benzene derivatives containing halogens and carboxyls: determination using the shake-flask method and estimation using the fragment method, J. Chem. Eng. Data 53 (2008) 280–282.
[19] R.E. Morris, R.E. Aird, P.D. Murdoch, H.M. Chen, J. Cummings, N.D. Hughes, et al., Inhibition of cancer cell growth by ruthenium(II) arene complexes, J. Med. Chem. 44 (2001) 3616–3621.
[20] J. Bernstein, R.E. Davis, L. Shimoni, N.L. Chang, Patterns in hydrogen bonding: functionality and graph set analysis in crystals, Angew. Chem. Int. Ed. 34 (1995) 1555–1573.
[21] R. Schuecker, R.O. John, M.A. Jakupec, V.B. Arion, B.K. Keppler, Water-soluble mixed-ligand ruthenium(II) and osmium(II) arene complexes with high antiproliferative activity, Organometallics 27 (2008) 6587–6595.
[22] Y.H. Zhao, M.H. Abraham, Octanol/water partition of ionic species, including 544 cations, J. Org. Chem. 70 (2005) 2633–2640.
[23] A. Pastuszko, K. Majchrzak, M. Czyz, B. Kupcewicz, E. Budzisz, The synthesis, lipophilicity and cytotoxic effects of new ruthenium(II) arene complexes with chromone derivatives, J. Inorg. Biochem. 159 (2016) 133–141.
[24] S. Bhattacharyya, K. Purkait, A. Mukherjee, Ruthenium(ii) p-cymene complexes of a benzimidazole-based ligand capable of VEGFR2 inhibition: hydrolysis, reactivity and cytotoxicity studies, Dalton Trans. 46 (2017) 8539–8554.
[25] I. Romero-Canelón, L. Salassa, P.J. Sadler, The contrasting activity of iodido versus chlorido ruthenium and osmium arene azo- and Imino-pyridine anticancer complexes: control of cell selectivity, cross-resistance, p53 dependence, and apoptosis pathway, J. Med. Chem. 56 (2013) 1291–1300.
[26] I. Romero-Canelon, A.M. Pizarro, A. Habtemariam, P.J. Sadler, Contrasting cellular

uptake pathways for chlorido and iodido iminopyridine ruthenium arene anticancer complexes, Metallomics 4 (2012) 1271–1279.
[27] L. Zhao, Q. Gu, L. Xiang, X. Dong, H. Li, J. Ni, L. Wan, G. Cai, G. Chen, Curcumin inhibits apoptosis by modulating Bax/Bcl-2 expression and alleviates oxidative stress in testes of streptozotocin-induced diabetic rats, Ther. Clin. Risk Manag. 13 (2017) 1099–1105.
[28] X. Wang, Z. Fu, Y. Chen, L. Liu, Fas expression is downregulated in gastric cancer, Mol. Med. Rep. 15 (2017) 627–634.
[29] H. Chen, X. Yang, Z. Feng, R. Tang, F. Ren, K. Wei, et al., Prognostic value of Caspase-3 expression in cancers of digestive tract: a meta-analysis and systematic review, Int. J. Clin. Exp. Med. 8 (2015) 10225–10234.
[30] Y. Sun, X.Y. Chen, J. Liu, X.X. Cheng, X.W. Wang, Q.Y. Kong, H. Li, Differential caspase-3 expression in noncancerous, premalignant and cancer tissues of stomach and its clinical implication, Cancer Detect. Prev. 30 (2006) 168–173.
[31] J. Kania, S.J. Konturek, K. Marlicz, E.G. Hahn, P.C. Konturek, Expression of survivin and caspase-3 in gastric cancer, Dig. Dis. Sci. 48 (2003) 266–271.
[32] M. Shintani, A. Sangawa, N. Yamao, S. Kamoshida, Smac/DIABLO expression in human gastrointestinal carcinoma: association with clinicopathological parameters and survivin expression, Oncol. Lett. 8 (2014) 2581–2586.
[33] L. Feng, M. Pan, J. Sun, H. Lu, Q. Shen, S. Zhang, et al., Histone deacetylase 3 inhibits expression of PUMA in gastric cancer cells, J. Mol. Med. 91 (2013) 49–58.
[34] V. Shoshan-Barmatz, N. Keinan, S. Abu-Hamad, D. Tyomkin, L. Aram, Apoptosis is regulated by the VDAC1 N-terminal region and by VDAC oligomerization: release of cytochrome c, AIF and Smac/Diablo, Biochim. Biophys. Acta 1797 (2010) 1281–1291.